Heliyon 9 (2023) e15128

Contents lists available at ScienceDirect

Heliyon

journal homepage: www.cell.com/heliyon

Research article

Nonlinear regression for treating adsorption isotherm data to characterize new sorbents: Advantages over linearization demonstrated with simulated and experimental data

Renan Vitek [a], Jorge C. Masini [b,*]

[a] Instituto Federal de Educação Ciência e Tecnologia de Mato Grosso, Cuiabá, Brazil
[b] Departamento de Química Fundamental, Instituto de Química, Universidade de São Paulo, Av. Prof. Lineu Pestes 748, 05508-000 São Paulo, SP, Brazil

ARTICLE INFO

Keywords:
Adsorption capacity
Adsorption affinity
Heterogeneity
Molecularly imprinted polymers
Mixed-mode interactions
Humic acid

ABSTRACT

This paper demonstrates that determining adsorption capacity and affinity through data fitting of adsorption isotherms by nonlinear regression (NLR) is more accurate than linearized Langmuir equations. Linearization errors and the subjective choice of data points used to apply the linear regression analysis may deviate the fitted adsorption parameters (constants and adsorption capacities) from the expected values. The deviation magnitude increases for heterogeneous sorbents such as environmental particles and molecularly imprinted polymers, which adsorb by more than one sorption mechanism or adsorption sites of diverse chemical natures. For instance, Lineweaver-Burk linearization of isotherms simulated considering the presence of two adsorption sites (distinct adsorption energies) provides excellent linear regression fittings but for only one kind of adsorption site. Contrary, Scatchard and Eadie-Hoffsiee's equations indicate the presence of more than one kind of adsorption site, but if the difference between the adsorption constants is not significant, the choice of points used to perform the computation becomes subjective. On the contrary, NLR analysis considers all the adsorption points (experimental or simulated), providing objective criteria to define if more than one kind of site or retention mechanism rules the adsorbed amounts of analyte. The fitted constants have smaller deviations from the expected values than those obtained by linearization. In addition to the simulated data, the enhanced robustness of the NLR was demonstrated in the determination of the adsorption capacity and adsorption affinity of a humic acid sample towards Cu^{2+} at different pH.

1. Introduction

Sorbents developed for solid-phase extraction (SPE) retain the analytes via a primary interaction mechanism (hydrophobic, hydrophilic, ion exchange, H-bond, complexation, molecular recognition). Secondary interactions may also control the sorption efficiency. Residual silanols are a classic example of this secondary interaction group in silica-based stationary phases designed to retain basic analytes in reversed-phase chromatography [1]. Mixed-mode sorbents have become common, especially those providing ion exchange and hydrophobic retention mechanisms [2,3]. Polymers with hydrophilic-lipophilic balance (HLB) are commercially available for SPE, providing hydrophilic interactions in N-vinylpyrrolidone groups, whereas divinylbenzene rings provide lipophilic

* Corresponding author.
E-mail address: jcmasini@iq.usp.br (J.C. Masini).

https://doi.org/10.1016/j.heliyon.2023.e15128
Received 8 June 2022; Received in revised form 24 March 2023; Accepted 27 March 2023
Available online 31 March 2023

interactions [4]. Molecularly imprinted polymers (MIP) have been extensively developed and often exhibit secondary interaction mechanisms in addition to molecular recognition [5–9].

One step in characterizing new sorbents is determining their adsorption capacity and affinity for the target compound. This characterization is usually made by constructing adsorption isotherms and fitting the data to Langmuir's equation (equation (1)) to determine the adsorption capacity (q_{max}) and the adsorption constant related to the variation of the Gibbs free energy ($K_{L.}$) [10].

$$q_e = q_{max}\frac{K_L c_e}{1 + K_L c_e} \tag{1}$$

Where q_e is the adsorbed amount of analyte per unit mass of the sorbent, and the c_e is the free concentration of the analyte in equilibrium with the sorbent. Despite the easy implementation of nonlinear regression analysis to investigate the fitting of the experimental data to adsorption models [11–13] and the advantages of this strategy demonstrated in several other works [14,15], several articles still describe the use the linearized forms of the Langmuir equation, such as those proposed by Hanes-Woolf (equation (2)), Lineweaver-Burk (equation (3)), Eadie -Hoffsiee (equation (4)) and Scatchard (equation (5)) [11].

$$\frac{c_e}{q_e} = \left(\frac{1}{q_{max}}\right)c_e + \frac{1}{q_{max}K_L} \tag{2}$$

$$\frac{1}{q_e} = \left(\frac{1}{q_{max}K_L}\right)\ \frac{1}{c_e} + \frac{1}{q_{max}} \tag{3}$$

$$q_e = -\frac{1}{K_L}\frac{q_e}{c_e} + q_{max} \tag{4}$$

$$\frac{q_e}{c_e} = -K_L q_e + K_L q_{max} \tag{5}$$

The Scatchard equation is the most used, especially for describing the adsorption properties of new MIPs. From equation (5), it is straightforward to deduce that the slope of the plot of $\frac{q_e}{c_e}$ vs. q_e provides the negative of K_L whereas the q_{max} can be obtained by dividing the intercept by the slope.

The main assumptions to the experimental data fit to Langmuir equation are: (i) there is a fixed number of adsorption sites available on the adsorbent surface and that these sites interact with the adsorbate with the same energy; (ii) the adsorption is reversible, (iii) the adsorption occurs as a monolayer, that is, once the adsorbate occupies one site no further adsorption occurs at that site, and (iv) no interaction occurs between adsorbate species.

Assumption (i) may not accurately describe the adsorption on adsorbents offering mixed-mode or secondary mechanisms. For polymers designed for molecular recognition mechanism, the imprinted polymer (MIP) is mainly characterized by two kinds of interaction sites, the strongest corresponding to molecular recognition cavities, whereas the weakest occur at nonspecific sites [16–22]. In an environmental context, humic substances control toxic metals' availability by adsorption in strong and weak sites. Whereas multidentate carboxylates, thiolated and amino carboxylate groups have a strong affinity but low capacity, single carboxylates and phenols exhibit low affinity and high adsorption capacities towards the metal ions [23].

A multi-site Langmuir adsorption isotherm [13,14] better describes the adsorption data of adsorbents interacting through more than one mechanism or distinct adsorption energies. Equation (6) shows a dual-sites Langmuir equation:

$$q_e = q_{max,1}\frac{K_{L,1}c_e}{1 + K_{L,1}c_e} + q_{max,2}\frac{K_{L,2}c_e}{1 + K_{L,2}c_e} \tag{6}$$

Indexes 1 and 2 refer to the two different kinds of adsorption sites (differing adsorption energies or K_L) whereas q_{max} and K_L have the same meaning defined in Equation (1).

If condition (i) of Langmuir's assumptions is not obeyed and the adsorption energy is not homogeneous due to the existence of sorption sites with different chemical natures governing the adsorption, the plot $\frac{q_e}{c_e}$ vs. q_e in the Scatchard plot is no longer linear, leading to computation errors [11]. The choice of points following some linear trend between $\frac{q_e}{c_e}$ and q_e suffer from subjectivity because equilibria in multi-site sorbents overlap.

Also, if Langmuir assumptions are not obeyed, the adsorption data may be well fitted to the empirical Freundlich equation in its nonlinear (equation (7)) and linearized forms (equation (8))

$$q_e = K_f c_e^n \tag{7}$$

$$log\ q_e = log\ K_F + n log\ c_e \tag{8}$$

where $K_{F.}$ is the Freundlich empirical constant ((mg kg^{-1})/(mg L^{-1})^n), and n is the dimensionless nonlinearity parameter associated with the energetic heterogeneity of the adsorption sites, lying between 0 and 1. The closer the n value is to the unity, the more homogeneous the adsorbent is, so the $K_{F.}$ approaches a Henry-like constant. The Freundlich equation, different from the Langmuir model, cannot describe the adsorption at high adsorbate concentrations close to the saturation of the adsorption sites. $K_{F.}$ can only be related to the maximum adsorption capacity (q_{max}) if n approaches infinity [11].

Mixed-mode interaction mechanisms assuming the existence of nonspecific interactions, such as partition-like mechanisms and specific interactions, can be described by the following equation:

$$q_e = K_H c_e + \frac{q_{max} K_L c_e}{1 + K_L c_e} \tag{9}$$

Where q_e, q_{max}, c_e, and $K_{L.}$ have the same meaning as equation (1), and $K_{.H.}$ is the Henry-like partition constant.

This paper demonstrates that fitting simulated and experimental adsorption data to single-site or dual-site Langmuir models and mixed-mode mechanisms is easily accessible by nonlinear regression with available software packages. This approach avoids the subjective choice of points demanded by linearized isotherms, providing more accurate and precise adsorption capacity and affinity estimations to characterize novel sorbents often proposed in the literature for applications in environmental remediation or solid phase extraction.

2. Methodology

2.1. Simulation parameters

Single-site isotherms were simulated with equation (1), assuming the arbitrary $q_{max} = 0.01$ mol g^{-1} and $K_L = 1.0 \times 10^5$ L g^{-1}. Using the dual-sites Langmuir equation (equation (6)), isotherms were simulated assuming the $q_{max,1} = 0.01$ mol g^{-1}, $K_{L,1} = 1.0 \times 10^5$ L g^{-1}, $q_{max,2} = 0.05$ mol g^{-1}, and $K_{L,2} = 1.0 \times 10^3$ L g^{-1}. For the hypothetical mixed-mode sorbent, equation (9) was used with a dimensionless Henry-like $K_H = 100$ together with the specific Langmuir site having $q_{max} = 0.01$ mol g^{-1} and $K_L = 1.0 \times 10^5$ L g^{-1}. All simulations were in a $1.0 \times 10^{-8} < c_e < 1.0 \times 10^{-3}$ mol L^{-1} range, and a random 2% error distribution was ascribed to the q_e values.

2.2. Experimental data – complexation of Cu^{2+} by humic acidd

In the complexation studies, 25.00 mL of a 30.0 mg L^{-1} acid humic acid suspension isolated from vermicompost was titrated with a 4.72 mmol L^{-1} Cu^{2+} keeping the ionic medium composed predominantly of 0.10 mol L^{-1} KNO_3. The range of total Cu^{2+} concentrations varied from 6.66×10^{-8} to 2.0×10^{-4} mol L^{-1}. The free concentrations of Cu^{2+} were measured using a 9429SC Cu^{2+} ion selective from Thermo Scientific Orion against a 3.0 mol L^{-1} KCl Ag/AgCl reference electrode model 405NS-S7/80 from Mettler Toledo and a Metrohm B654 potentiometer. The titrations were made at 25.0 ± 0.1 °C and pH 4.0, 5.0 and 6.0. The free and bound concentrations of Cu^{2+} were designed as [Cu^{2+}] and [CuL], respectively, with mol L^{-1} units. More detailed information on the samples and techniques is given elsewhere [24,25].

2.3. Fitting

All the simulations and fittings were made using the Origin 2020 64-bit Academic software (OriginLab Corporation, Northampton, MA, USA). One-site Langmuir and Freundlich equations were in the library of equations as Power Origin Functions. The codes of two-sites and Partition-Langmuir were quickly added to the equations library. Fittings were made by using the Levenberger-Marquardt iteration algorithm. The maximum number of iterations and tolerance were 400 and 1×10^{-9} as the software's default.

Unlike linearization methods, NLR fitting depends on initial values to start the iterative computation. The initial value of q_{max} can be easily estimated from the adsorption isotherm, especially if the q_e reaches a plateau at higher values of c_e. For the other parameters, we used the trial and error approach. If the estimated initial value significantly deviates from the "correct" value, the computation results in negative parameters (no physical meaning) or error messages the software provides due to a lack of fitting.

The fitting quality of the models was tested by calculating the coefficient of determination (R^2, equation (10)) and the chi-squared parameter (χ^2) (equation (11)).

$$R^2 = 1 - \frac{\sum \left(q_{e,exp} - q_{e.calc}\right)^2}{\sum \left(q_{e,exp} - q_{e,mean}\right)^2} \tag{10}$$

$$\chi^2 = \sum \frac{\left(q_{e,exp} - q_{e,calc}\right)^2}{q_{e,calc}} \tag{11}$$

Where $q_{e,exp}$ is the experimental (or simulated) value of q, measured at equilibrium, $q_{e,calc}$ is the fitted value of q, and $q_{e,mean}$ is the mean value of experimental (or simulated) q. The closer R^2 is to the unity, the better the fitting quality. In equations (10) and (11), if $q_{e,calc}$ using a model is similar to the $q_{e,exp}$, χ^2 is close to zero. High χ^2 values indicate a high bias between the experimental data and the tested model.

Another validation tool was the ($q_{e,exp} - q_{e,calc}$) versus c_e plot, also known as the residual plots. For a good model, the residuals should distribute randomly and normally as a function of c_e [26].

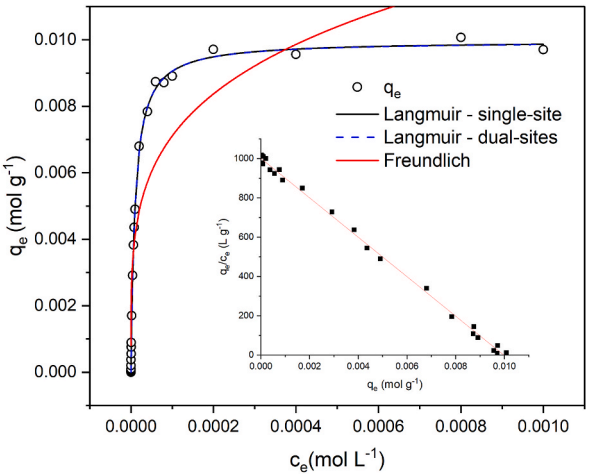

Fig. 1. Simulated adsorption isotherm assuming one specific adsorption site following the Langmuir equation (Equation (1)) and the corresponding trending lines obtained by fitting the data by single-site, dual-sites Langmuir and Freundlich equations. The inset shows the data linearization by the Scatchard equation (equation (5)).

Table 1
Langmuir parameters used to simulate adsorption isotherms and the fitted parameters using Scatchard Equation and Nonlinear Regression Fitting (NLR).

Adsorption and Fitting Parameters	Simulated Values	Fitted Values		
		Scatchard	Nonlinear Regression	
			Single-site	Dual-site
$K_{L,1}$ (L g^{-1})	1.0×10^5	$(9.2 \pm 0.3) \times 10^4$	–	$(10._5 \pm 1._4) \times 10^4$
$K_{L,2}$ (L g^{-1})	1.0×10^3	$(1.43 \pm 0.02) \times 10^3$	$(2.2 \pm 0.3) \times 10^3$	$(1.05 \pm 0.05) \times 10^3$
$q_{max,1}$ (mol g^{-1})	0.010	0.0114 ± 0.0002	–	0.0098 ± 0.0005
$q_{max,2}$ (mol g^{-1})	0.050	0.048 ± 0.002	0.057 ± 0.002	0.0495 ± 0.0005
$q_{max,\ total}$ (mol g^{-1})	0.060	0.059 ± 0.002	0.057 ± 0.002	0.059 ± 0.001
χ^2	–	–	7.9×10^{-6}	1.97×10^{-7}
R^2	–	0.9999 (site 1) 0.998 (site 2)	0.98	0.999

3. Results and discussion

3.1. Single-site adsorbent

The simplest case is the sorbent following the single-site Langmuir model, illustrated in Fig. 1 for a data set simulated assuming $K_{L.} = 1.0 \times 10^5$ L g^{-1} and $q_{max} = 0.01$ mol g^{-1} with random 2% error in q_e. Applying the Scatchard equation to the simulated data returned $K_L = (1.00 \pm 0.01) \times 10^5$ L g^{-1} and $q_{max} = (9.96 \pm 0.06) \times 10^{-2}$ mol g^{-1}, with $R^2 = 0.997$ (inset in Fig. 1). Fitting data by NLR with the single-site Langmuir equation returned fitted parameters not significantly different from those provided by linearization ($K_L = 1.01 \pm 0.02) \times 10^5$ L g^{-1}, and $q_{max} = (9.96 \pm 0.05) \times 10^{-2}$ mol g^{-1}, with $R^2 = 0.9992$ and $\chi^2 = 1.34 \times 10^{-8}$). The dual-sites Langmuir model also provided an excellent fitting ($R^2 = 0.9992$ and $\chi^2 = 1.40 \times 10^{-8}$). The fitted parameters for the strongest site (site 1) agreed with the values used to simulate the isotherm. However, for the weakest site (site 2), both $K_{L.}$ and q_{max} were negative, showing that the dual-site model, although providing an excellent overlap between the fitted and simulated curves (Fig. 1) and random residual distribution (Fig. S1), returns meaningless K_L and q_{max} parameters. Thus, there is no clear advantage in using NLR over the Scatchard linearization for the single-site sorbent, also characterized by a clear plateau indicating the sorbent saturation at high c_e values (>0.2 mmol L^{-1} in Fig. 1).

The Freundlich equation did not provide a good fit in the $10^{-8} > c_e > 10^{-3}$ mol L^{-1} ($R^2 = 0.86$, Fig. 1), resulting, for instance, $1/n = 0.24 \pm 0.03$, which is not consistent with a high energetic homogeneity since only one kind of adsorption site is assumed in the simulation. The computation restricting the c_e range between 10^{-8} and 10^{-5} mol L^{-1} improved the fitting ($R^2 = 0.994$, $\chi^2 = 2.0 \times 10^{-8}$), resulting in $1/n = 0.72 \pm 0.03$, which is more consistent with the energetic homogeneity. This finding is also consistent with the inadequacy of the Freundlich equation to model the isotherm in the site saturation region. Fitting data in different ranges of site occupation and obtaining different Freundlich parameters indicates that the model is unsuitable for data modeling.

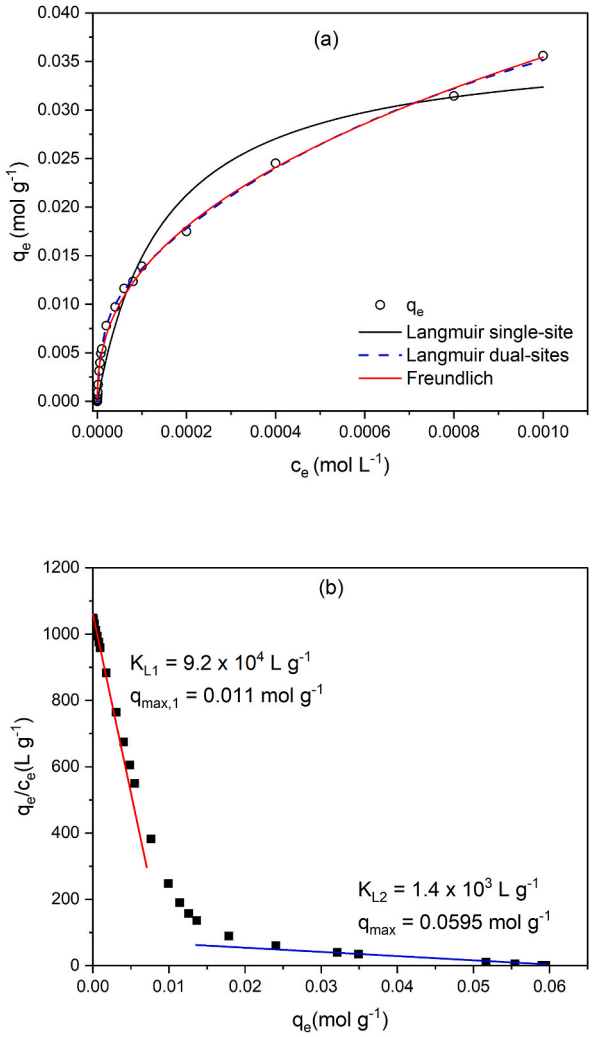

Fig. 2. (a) Simulated adsorption isotherm assuming the presence of two specific adsorption sites following the Langmuir equation (Equation (6)) and the corresponding trending lines obtained by fitting the data with single-site and dual-sites Langmuir and the Freundlich equations. (b) Scatchard plot resulting from applying the model to the simulated adsorption data shown in (a).

3.2. Dual-site adsorbents

This section addresses adsorbents having two kinds of adsorption sites with different constants and capacities, arbitrarily chosen. Site 1 was a strong affinity site ($K_{L,1} = 1.0 \times 10^5$ L g^1) with low capacity (0.010 mol g^{-1}), and site 2 was less energetic ($K_{L,2} = 1.0 \times 10^3$ L g^{-1}) but having a greater capacity of 0.050 mol g^{-1} (Table 1).

Treating the simulated isotherm (Fig. 2a) with the Scatchard equation suggests the existence of two kinds of adsorption sites since the $\frac{q_e}{c_e}$ vs. q_e plot exhibits a change in slope (Fig. 2b). A visual analysis of the graph shows that it is straightforward to choose q_e up to 5 mmol g^{-1} to apply the linear regression analysis corresponding to the stronger affinity site. From this linear portion, it was possible to estimate $q_{max,1} = 0.0114 \pm 0.0001$ and $K_{L,1} = (9.2 \pm 0.3) \times 10^4$ L g^{-1}, which correspond to +10 and −8% deviation relative to the expected values (Table 1). For q_e values between 0.03 and 0.06 mol g^{-1}, it is possible to find a linear relationship with $R^2 = 0.998$, producing a $K_{L,2} = (1.43 \pm 0.02) \times 10^3$ L g^{-1} (Table 1), having a 43% deviation from the expected value, and a $q_{max,2} = 0.048 \pm 0.002$ mol g^{-1}, with a −3.8% deviation from the expected value and a deviation of −0.83% regarding the sum of capacities of sites 1 and 2. Although the fitted parameters are in good agreement with the expected values, they can change significantly, especially site 2, because $\frac{q_e}{c_e}$ values do not change linearly with q_e. Finding a concentration range without equilibria overlapping between sites 1 and 2 requires many data points at high c_e, implying the necessity of an analytical method with a wide linear dynamic range or extensive dilutions [27], which may cause experimental errors in the measurements.

The NLR uses all the data points in the fitting, thus eliminating the subjective choice of points to be included or excluded from the regression analysis (as in linearization). In a real-life experiment, one does not know *a priori* how many kinds of adsorption sites exist in

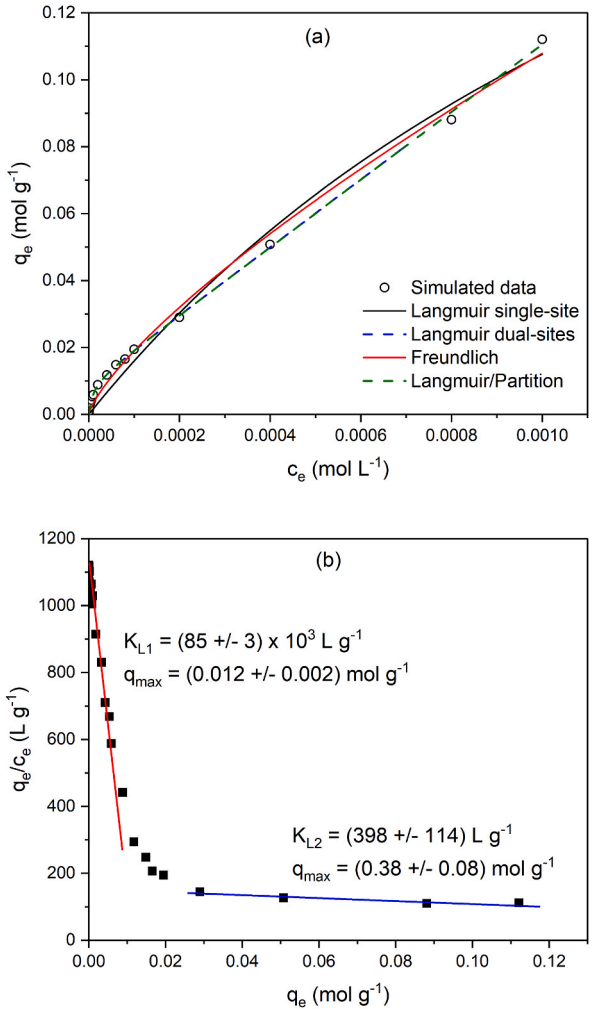

Fig. 3. (a) Simulated adsorption isotherm assuming the presence of mixed-mode adsorption sites following the Langmuir (specific) and partition (unspecific) interaction mechanism (Equation (9)) and the corresponding trending lines obtained by fitting the data by single-site, dual-sites Langmuir and Freundlich equations, as well as by the Langmuir-Partition model. (b) Linearization by the Scatchard equation of the simulated adsorption data.

Table 2
Langmuir/partition parameters used to simulate adsorption isotherms and the fitted parameters using Scatchard Equation and Nonlinear Regression Fitting (NLR).

Adsorption and Fitting Parameters	Simulated Values	Fitted Values			
		Scatchard	Nonlinear Regression		
			1-site	2-site	Langmuir-Partition
K_H	100	–	–	–	101.0 ± 0.8
$K_{L,1}$ (L g^{-1})	1.0×10^5	$(85 \pm 3) \times 10^3$	–	$(1.1 \pm 0.2) \times 10^5$	$(1.1 \pm 0.2) \times 10^5$
$K_{L,2}$ (L g^{-1})	–	$(4 \pm 1) \times 10^2$	$(6 \pm 1) \times 10^2$	27 ± 263	–
$q_{max,1}$ (mol g^{-1})	0.010	0.013 ± 0.002	–	$(9.7 \pm 0.7) \times 10^{-3}$	$(9.7 \pm 0.7) \times 10^{-3}$
$q_{max,2}$ (mol g^{-1})	–	0.37 ± 0.08	0.30 ± 0.05	4 ± 35	–
$q_{max,\ total}$ (mol g^{-1})	0.010	0.38 ± 0.08	0.30 ± 0.05	4 ± 35	$(9.7 \pm 0.7) \times 10^{-3}$
χ^2	–	–	9.8×10^{-6}	4.2×10^{-7}	3.98×10^{-7}
R^2	–	0.98 (site 1) 0.86 (site 2)	0.98	0.999	0.999

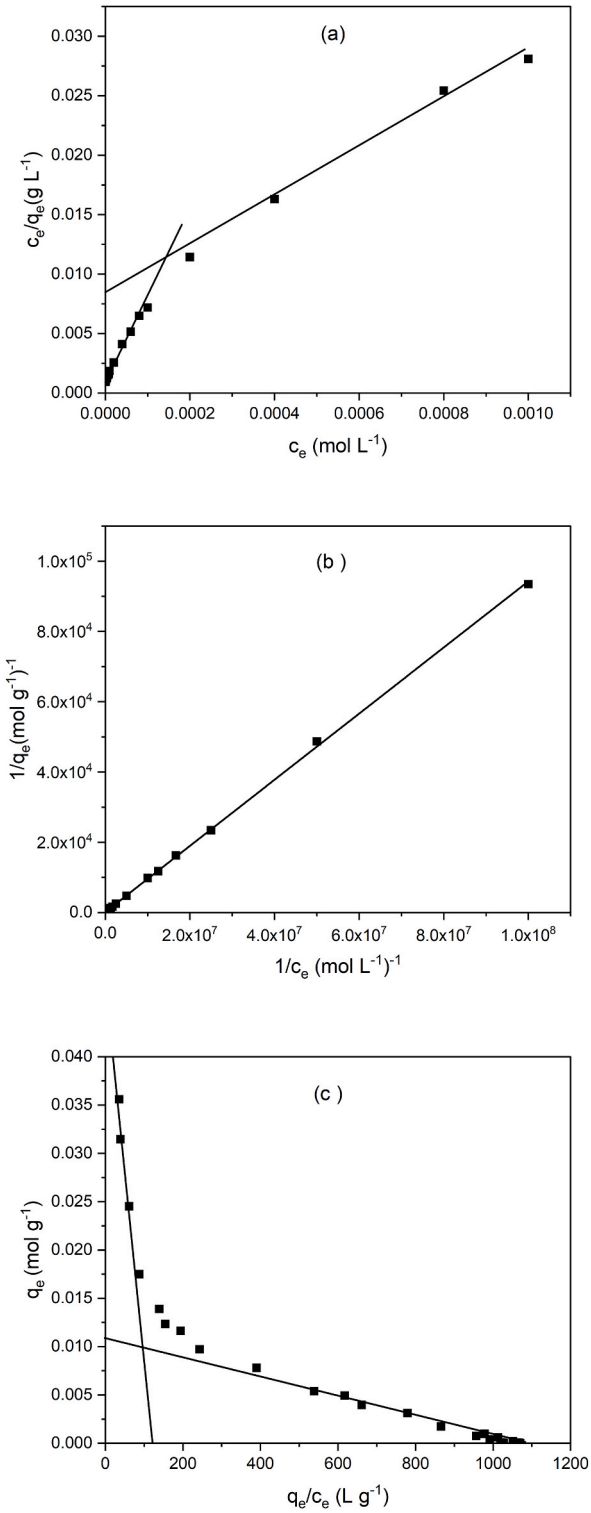

Fig. 4. Linearized adsorption isotherms using (a) Hanes-Woolf (H–W), (b) Lineweaver-Burk (L–B), and (c) Eadie-Hofsiee (E–H) equations applied to simulated data considering dual-sites adsorbent following the multi-site Langmuir isotherm, assuming $q_{max,1} = 0.010$; $q_{max,2} = 0.050$ mol g^{-1} $K_{L,1} = 1.0 \times 10^5$ L mol^{-1}, and $K_{L,2} = 1.0 \times 10^3$ L mol^{-1}.

Table 3
Simulated and fitted adsorption parameters obtained by using Hanes-Woolf (H–W), Lineweaver-Burk (L-B), and Eadie-Hofsiee (E-H) linearization equations.

Adsorption and Fitting Parameters	Simulated Values	Fitted Values		
		Linearization Model		
		H–W	L-B[a]	E-H
$K_{L,1}$ (L g^{-1})	1.0×10^5	$(9.0 \pm 0.3) \times 10^4$	1.44×10^5	$(9.4 \pm 0.9) \times 10^5$
$K_{L,2}$ (L g^{-1})	1.0×10^3	$(5.4 \pm 0.7) \times 10^3$		$(3.1 \pm 0.3) \times 10^3$
$q_{max,1}$ (mol g^{-1})	0.010	$(1.12 \pm 0.04) \times 10^{-2}$	–	0.0112 ± 0.0003
$q_{max,2}$ (mol g^{-1})	0.050	0.040 ± 0.002	–	0.046 ± 0.002
$q_{max,\ total}$ (mol g^{-1})	0.060	0.051 ± 0.04	$(7.36 \pm 12) \times 10^{-3}$	0.057 ± 0.002
R^2	–	0.98 (site 1)	0.999	0.97 (site 1)
		0.98 (site 2)		0.985 (site 2)

[a]L-B linearization does not show slope changes suggesting only a single site controls the adsorption. Thus, it is impossible to assign K_L and q_{max} to sites 1 or 2.

the studied sorbent. Thus, different models must be investigated to find the one best describes the experimental data. Assuming the presence of only one kind of adsorption site, the NLR provides an acceptable fitting ($R^2 = 0.99$ and $\chi^2 = 7.9 \times 10^{-6}$), returning $q_{max} = 0.057 \pm 0.002$ mol g^{-1}, implying in a −5% deviation from the expected 0.060 mol g^{-1} value. The fitted $K_{L.}$ $(2.2 \pm 0.3) \times 10^3$ L g^{-1} corresponds to roughly a mean of the $K_{L.}$ values weighted by their respective abundances. A closer look at the fitted line using the single-site model shows significant deviations between simulated and fitted q_e values in the c_e range between 0.1 and 0.9 mmol L^{-1} (Fig. 2a), also evidenced in the waved distribution of residuals (Fig. S2a).

Fitting the data to the dual-sites isotherms returned q_{max} of $(9.8 \pm 0.5) \times 10^{-3}$ and $(4.95 \pm 0.05) \times 10^{-2}$ mol g^{-1} for the sites 1 and 2, respectively. The sum of these q_{max} values results (0.059 ± 0.001) mol g^{-1}, in excellent agreement with the expected total capacity (Table 1). The $K_{L.}$ values deviated by 4.6 and 5.3% from the expected constants (Table 1). Compared to the fitting with only one kind of adsorption site, a significant improvement of R^2 to 0.999 and χ^2 to 1.96×10^{-7} confirmed the dual-sites model best fitting the simulated data. The residual plot (Fig. S2b) shows a random distribution of errors, different from the residual plot for the single-site fitting (Fig. S2a). Adding a third kind of adsorption site does not lead to fitting, thus confirming that the dual-sites model is the right choice to estimate the adsorption capacity and affinity.

The Freundlich equation provides an excellent fit up the c_e of about 1 mmol L^{-1} (Fig. 2a), with $R^2 = 0.996$ and $\chi^2 = 4.3 \times 10^{-7}$, resulting $K_F = 0.65 \pm 0.04$ (mol/g)/(mol/L)^n and $1/n = 0.422 \pm 0.009$. The $K_{F.}$, however, is not a proper parameter to estimate the maximum adsorption capacity, but the 1/n value < 1 confirms the high heterogeneity of the adsorbent, consistent with the two kinds of adsorption sites. The Freundlich model fails to model the data as the site saturation approaches ($c_e > 0.001$ mol L^{-1}, not shown), so this model is unsuitable for determining q_{max}.

3.3. Mixed-mode adsorbent exhibiting specific and nonspecific sorption sites

In this section, the adsorption isotherm simulated a hypothetical adsorbent containing one kind of specific adsorption site following the Langmuir equation with $K_{L.} = 1.0 \times 10^5$ L g^{-1} and $q_{max} = 0.01$ mol g^{-1}, together with a partition mechanism following a Henry-like dimensionless partition constant (equation (9)) with an arbitrary value of 100 (Fig. 3a).

Linearizing the data by the Scatchard equation indicates (Fig. 3b) the presence of two kinds of adsorption sites/mechanisms. However, only the parameters relative to the specific site with a greater affinity for the analyte fit the data reasonably. The values of $q_{max,\ 1}$ and $K_{L,1}$ were 0.012 ± 0.002 mol g^{-1} and $(85 \pm 3) \times 10^3$ L g^{-1}, respectively, implying +20% deviation in $q_{max,1}$ and −15% in $K_{L.,1}$, with an $R^2 = 0.98$ (Table 2), usually accepted as a "good" or acceptable fitting for these modeling. The data corresponding to the second kind of adsorption site suggested by the Scatchard plot indeed does not fit the model, exhibiting a poor $R^2 = 0.86$ and fitting parameters without any correspondence with the values used to simulate the isotherm, especially if one considers the q_{max}, that is meaningless for a partition model.

Fitting data by NLR by the single-site Langmuir model provided $R^2 = 0.98$ and $\chi^2 = 9.8 \times 10^{-6}$, resulting $q_{max} = 0.30 \pm 0.05$ mol g^{-1} and $K_L = (6 \pm 1) \times 10^2$. Although R^2 and χ^2 suggest the model provided a good fitting, the fitted parameters do not correspond to the values used to simulate the isotherm. The fitting to the dual-sites Langmuir model did not converge, but the software returns "fitted" parameters after the predefined 400 iterations (Table 2) with high R^2 and low χ^2 values. However, whereas the fitted parameters for site 1 correspond well with the values used to simulate the isotherm, the parameters for site 2 were just numerical values providing a good fitting. The standard deviations higher than the fitted values for site 2 (Table 2), and the lack of fitting convergence, confirm the physical meaningless of the found numbers for "site 2" and the inadequacy of the dual-sites Langmuir model to describe the simulated isotherm.

As expected, fitting the data to the Langmuir-partition model (equation (9)) provides excellent R^2 and χ^2 values, with a $K_{H.}$ exhibiting only a 1% deviation from the expected value. The specific-high affinity site (following the Langmuir model) exhibited a −3% deviation in q_{max} and +10% in K_L (Table 2). Another evidence of the two mechanisms ruling the adsorption is the isotherm shape, which at low c_e values exhibits an L-type shape in the Giles classification [28], typical of situations following the Langmuir assumptions. As c_e increases, the isotherm shape changes to a C-type, typical of the partition mechanism.

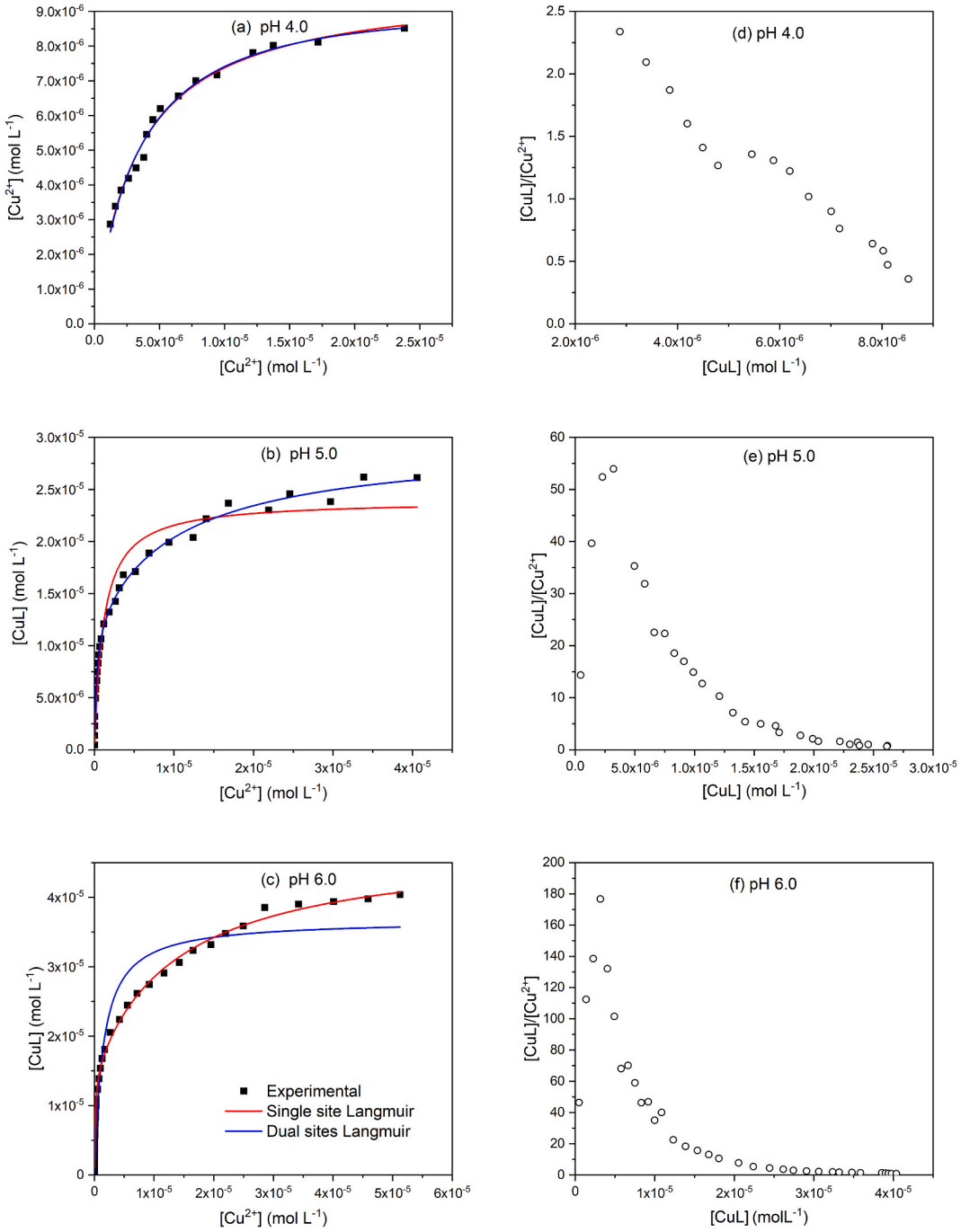

Fig. 5. Experimental adsorption of Cu^{2+} on humic acid at (a) pH 4.0, (b) 5.0 and (c) 6.0 measured at 25.0 ± 0.1 °C fitted by NLR (left panel) assuming single- and dual-site Langmuir equations and linearized by the Scatchard equation for the data corresponding to (d) pH 4.0, (e) pH 5.0 and (f) pH 6.0 (right panel).

Fitting the simulated data to the Freundlich equation provided good $R^2 = 0.996$ and $\chi^2 = 3.8 \times 10^{-6}$, consistent with the heterogeneity of adsorption sites assumed in this model. For the c_e window between 1×10^{-8} and 1×10^{-3} mol L^{-1} fitted K_F (20 ± 3) (mol/g)/(mol/L)^n and $1/n = 0.76 \pm 0.02$. However, these values are extremely dependent on the concentration range used for the computation. For instance, if the upper c_e is limited to 2.0×10^{-4} mol L^{-1} the returned $K_F = 3.3 \pm 0.3$ (mol/g)/(mol/L)^n and $1/n = 0.56 \pm 0.01$. The $1/n < 1$ is consistent with the heterogeneity of the adsorption sites, and the increase of $1/n$ for using c_e up to 1×10^{-3} mol L^{-1} instead 2×10^{-4} mol L^{-1} is explained by the enhanced participation of the partition mechanism modeling the data set.

Table 4
Adsorption capacities and constants for the interaction of Cu^{2+} with humic acid (30 mg L^{-1}) at 25.0 ± 0.1 °C determined by NLR and Scatchard plot.

pH	Parameter[a]	NLR	Scatchard
	$q_{max} \times 10^4$ (mol g^{-1})	3.25 ± 0.06	3.2 ± 0.3
4.0	Log K_L	5.49 ± 0.03	5.49 ± 0.02
	R^2	0.98	0.95
	χ^2	4.27×10^{-14}	–
5.0	$q_{max,1} \times 10^4$ (mol g^{-1})	4.1 ± 0.3	$3._7 \pm 1._0$
	Log $K_{L,1}$	6.606 ± 0.009	6.79 ± 0.05
	$q_{max,2} \times 10^4$ (mol g^{-1})	5.8 ± 0.3	$5._3 \pm 1._3$
	Log $K_{L,2}$	5.98 ± 0.01	5.53 ± 0.05
	$\Sigma q_{max} \times 10^4$	9.9 ± 0.6	9 ± 2
	R^2	0.995	0.91 (Site 1); 0.85 (Site 2)
	χ^2	3.38×10^{-13}	–
6.0	$q_{max,1} \times 10^4$ (mol g^{-1})	5.0 ± 0.2	3.0 ± 0.2
	Log $K_{L,1}$	6.88 ± 0.05	6.43 ± 0.08
	$q_{max,2} \times 10^3$ (mol g^{-1})	1.09 ± 0.03	1.2 ± 0.3
	Log $K_{L,2}$	4.86 ± 0.04	5.19 ± 0.02
	$\Sigma q_{max} \times 10^3$	1.6 ± 0.2	1.5 ± 0.3
	R^2	0.997	0.89 (site 1); 0.98 (site 2)
	χ^2	4.93×10^{-13}	–

a The q_{max} values were obtained by dividing the maximum complexation capacity (mol L^{-1}. shown in the y-axis of Fig. 5) by the humic acid concentration (0.030 g L^{-1}).

3.4. Hanes-Woolf (H–W), Lineweaver-Burk (L-B), and Eadie-Hofsiee (E-H) linearization

The dual-sites adsorption isotherm simulated with equation (6) (Fig. 2) was linearized by equations (2)–(4), and the Scatchard equation (equation (5)), as discussed in section 3.2. The plots appear in Fig. 4, and the fitted parameters are in Table 3. The H–W and E-H linearization indicate the presence of two adsorption sites, as in the Scatchard plot, by the significant slope change in the graphs of $\frac{c_e}{q_e}$ vs. c_e (H–W plot) and q_e vs. $\frac{q_e}{c_e}$ (E-H plot).

However, the L-B plot does not indicate that the two-sites model controls the adsorption (Fig. 4). Choosing linear portions in H–W and E-H plots seems more subjective than in the Scatchard plots, as evidenced by $R^2 < 0.99$ (Fig. 4, Table 3). Thus, +12, −14 and −5% deviations appeared in $q_{max,1}$, $q_{max,2}$, and $q_{max,\ total}$ in the E-H linearization (Table 3). Considering the E-H linearization, the errors were +12, −20 and −14.7% in $q_{max,1}$, $q_{max,2}$, and $q_{max,\ total}$, respectively.

The adsorption constants also exhibit significant deviations from the expected values (Table 3) since in both H–W and E-H equations, they are computed from the intercepts, so relying on extrapolation of straight lines fitted with poor linear correlation coefficients ($R^2 < 0.99$).

3.5. Experimental data for the titration of humic acid with Cu^{2+}

Nonlinear regression and linearization (Scatchard) analyses were applied to the adsorption of Cu^{2+} onto a suspension of vermicompost humic acid at pH 4.0, 5.0 and 6.0 (Fig. 5). At pH 4.0, the Scatchard plot is linear for all the experimental measurements indicating that the single-site Langmuir model describes the data. Nonlinear regression analysis using single and dual-site equations provided undistinguishable fitted lines (Fig. 5) but with the dual site's model returning negative values of adsorption capacity and constants, thus confirming that the single-site model is the one modeling the adsorptions. The residual plots (Fig. S3) were also indistinguishable at pH 4.0. The log K and q_{max} obtained by NLR and Scatchard plots were in good agreement, with the NLR approach providing better fitting parameters and a q_{max} with a lower standard deviation (Table 4), consistent with the simulation studies.

At pH 5.0 and 6.0, the NLR and Scatchard plots suggest the existence of two kinds of adsorption sites, consistent with the decreased competition of protons with Cu^{2+} and increased availability of binding sites in the humic substance, as revealed by the enhanced adsorption capacities. The random error distribution in the residual plots from the NLR analysis also indicates that the dual-sites equation better models the experimental data (Fig. S3). For the NLR analysis, all the experimental points were considered for the fitting, whereas the Scatchard plots clearly demand the exclusion of three to four points with the lower [CuL] values since they are not obeying the linearized equation. Choosing the points to fit the Scatchard equation is never without some degree of subjectivity because, rigorously, there are no purely linear regions in the plots. Consequently, the R^2 is always much worse than those found by NLR (Table 4), and the q_{max} values, which are determined by extrapolation to the y-axis, exhibit relative standard deviation around 20–30%, much higher than those obtained by NLR, especially at pH 5.0 (Table 4).

The H–W, L-B, and E-H plots (Fig. S4) at pH 4 provide a suitable linearization consistent with the single-site Langmuir model. At pH 5.0 and 6.0, the H–W plot exhibits a slight curvature indicating the existence of two kinds of adsorption sites, but without an additional statistical tool, such as the analysis of residual plots, the adsorption isotherm could be easily assumed as a single-site model. The L-B model was unsuitable since no linear region enables a reliable computation. The E-F equation performed similarly to the Scatchard model, requiring the exclusion of some experimental points but pointing to the existence of two kinds of adsorption sites.

4. Conclusion

Nonlinear regression analysis provides more accurate values and robust criteria to decide if single- or dual-sites control the adsorption isotherm. Additionally, NLR helps decide if mixed-mode mechanisms rule the adsorption. Although it is well known that linearization of nonlinear equations may result in errors in the fitted parameter, the present paper demonstrated quantitatively through simulations the magnitude of these errors in the adsorption capacities and adsorption constants fitted by linearization. Experimental data for the adsorption of Cu^{2+} by humic acid were consistent with the trends observed with the simulated data. In summary, NLR should be preferred to the linearized Scatchard, L-B, H–W or E-H equations to accurately characterize new SPE sorbents' adsorption capacities and adsorption affinities.

Declarations

Conflict of interest

The authors declare that they have no conflict of interest.

Author contribution statement

Jorge C. Masini: Conceived and designed the experiments; Analyzed and interpreted the data; Contributed reagents, materials, analysis tools or data; Wrote the paper.

Renan Vitek: Performed the experiments; Analyzed and interpreted the data; Wrote the paper.

Data availability statement

Data will be made available on request.

Acknowledgments

Research on solid-phase extraction has been funded by grants 2013/18507−4 from the São Paulo Research Foundation (FAPESP) and 306674/2021-1 from the National Council for Scientific and Technological Development (CNPq). Renan Vitek acknowledges Coordination for the Improvement of Higher Education Personnel (CAPES) for a Ph.D. fellowship (Contract 88887.499941/2020-00).

Appendix A. Supplementary data

Supplementary data to this article can be found online at https://doi.org/10.1016/j.heliyon.2023.e15128.

References

[1] C. Stella, S. Rudaz, M. Mottaz, P.A. Carrupt, J.L. Veuthey, Analysis of basic compounds at high pH values by reversed-phase liquid chromatography, J. Separ. Sci. 27 (2004) 284–292, https://doi.org/10.1002/jssc.200301671.

[2] S. Knoll, T. Rösch, C. Huhn, Trends in sample preparation and separation methods for the analysis of very polar and ionic compounds in environmental water and biota samples, Anal. Bioanal. Chem. 412 (2020) 6149–6165, https://doi.org/10.1007/s00216-020-02811-5.

[3] M.S. Mills, E.M. Thurman, M.J. Pedersen, Application of mixed-mode, solid-phase extraction in environmental and clinical chemistry. Combining hydrogen-bonding, cation-exchange and Van der Waals interactions, J. Chromatogr. A 629 (1993) 11–21, https://doi.org/10.1016/0021-9673(93)80349-D.

[4] I. Karki, P. Li, E.C. Vik, A. Manzewitsch, E. Divirgilio, W.E. Brewer, K.D. Shimizu, Absorption properties of monolithic poly (divinylbenzene-co-N-vinylpyrrolidone) over a wide range of monomer ratios, React. Funct. Polym. 163 (2021), https://doi.org/10.1016/j.reactfunctpolym.2021.104888.

[5] H.T. Nguyen, N.T. Vuong Bui, W.G. Kanhounnon, K.L. Vu Huynh, T.-V.-A. Nguyen, H.M. Nguyen, M.H. Do, M. Badawi, U.D. Thach, Co-precipitation polymerization of dual functional monomers and polystyrene- co -divinylbenzene for ciprofloxacin imprinted polymer preparation, RSC Adv. 11 (2021) 34281–34290, https://doi.org/10.1039/d1ra05505d.

[6] D. Deng, Y. He, M. Li, L. Huang, J. Zhang, Preparation of multi-walled carbon nanotubes based magnetic multi-template molecularly imprinted polymer for the adsorption of phthalate esters in water samples, Environ. Sci. Pollut. Res. 28 (2021) 5966–5977, https://doi.org/10.1007/s11356-020-10970-2.

[7] N. Mpayipheli, A. Mpupa, P.N. Nomngongo, Vortex-assisted dispersive molecularly imprinted polymer-based solid phase extraction of acetaminophen from water samples prior to hplc-dad determination, Separations 8 (2021), https://doi.org/10.3390/separations8100194.

[8] N. Surapong, R. Burakham, Magnetic molecularly imprinted polymer for the selective enrichment of glyphosate, glufosinate, and aminomethylphosphonic acid prior to high-performance liquid chromatography, ACS Omega 6 (2021), 27007, https://doi.org/10.1021/acsomega.1c03488. –27016.

[9] S. Zahara, M.A. Minhas, H. Shaikh, M.S. Ali, M.I. Bhanger, M.I. Malik, Molecular imprinting-based extraction of rosmarinic acid from Salvia hypoleuca extract, React. Funct. Polym. 166 (2021), 104984, https://doi.org/10.1016/j.reactfunctpolym.2021.104984.

[10] I. Langmuir, The adsorption of gases on plane surfaces of glass, mica and platinum, J. Am. Chem. Soc. 40 (1918) 1361–1403.

[11] H.N. Tran, S.J. You, A. Hosseini-Bandegharaei, H.P. Chao, Mistakes and inconsistencies regarding adsorption of contaminants from aqueous solutions: a critical review, Water Res. 120 (2017) 88–116, https://doi.org/10.1016/j.watres.2017.04.014.

[12] C.H. Bolster, G.M. Hornberger, On the use of linearized Langmuir equations, Soil Sci. Soc. Am. J. 71 (2007) 1796–1806, https://doi.org/10.2136/sssaj2006.0304.

[13] D.A. Castro, M. Milhomem, D. Pereira, P. Leal, Gurupi isotherms plot (GIP): a tool with intuitive and free graphic interface as an alternative for the calculation of adsorption isotherm parameters, Quim. Nova 44 (2021) 1028–1035, https://doi.org/10.21577/0100-4042.20170752.

[14] R. Sahin, K. Tapadia, Comparison of linear and non-linear models for the adsorption of fluoride onto geo-material: limonite, Water Sci. Technol. 72 (2015) 2262–2269, https://doi.org/10.2166/wst.2015.449.
[15] É.C. Lima, M.A. Adebayo, F.M. Machado, Kinetic and equilibrium models of adsorption, in: C.P. Bergmann, F.M. Machado (Eds.), Carbon Nanostructures as Adsorbents Environ. Biol. Appl., Springer, Cham, 2015, pp. 33–69, https://doi.org/10.1007/978-3-319-18875-1_3.
[16] D. Qin, J. Wang, C. Ge, Z. Lian, Fast extraction of chloramphenicol from marine sediments by using magnetic molecularly imprinted nanoparticles, Microchim. Acta 186 (2019), https://doi.org/10.1007/s00604-019-3548-9.
[17] P. Dramou, P. Zuo, H. He, L.A. Pham-Huy, W. Zou, D. Xiao, C. Pham-Huy, Development of novel amphiphilic magnetic molecularly imprinted polymers compatible with biological fluids for solid phase extraction and physicochemical behavior study, J. Chromatogr. A 1317 (2013) 110–120, https://doi.org/10.1016/j.chroma.2013.07.075.
[18] D. Zhao, J. Jia, X. Yu, X. Sun, Preparation and characterization of a molecularly imprinted polymer by grafting on silica supports: a selective sorbent for patulin toxin, Anal. Bioanal. Chem. 401 (2011) 2259–2273, https://doi.org/10.1007/s00216-011-5282-y.
[19] S. Chen, J. Fu, Z. Fu, Y. Li, X. Su, L. Zou, L. He, S. Liu, X. Ao, Y. Yang, Preparation and characterization of magnetic molecular imprinted polymers with ionic liquid for the extraction of carbaryl in food, Anal. Bioanal. Chem. 412 (2020) 1049–1062, https://doi.org/10.1007/s00216-019-02330-y.
[20] H. Fu, W. Xu, H. Wang, S. Liao, G. Chen, Preparation of magnetic molecularly imprinted polymer for selective identification of patulin in juice, J. Chromatogr., B: Anal. Technol. Biomed. Life Sci. 1145 (2020), https://doi.org/10.1016/j.jchromb.2020.122101.
[21] S. Tan, H. Yu, Y. He, M. Wang, G. Liu, S. Hong, F. Yan, Y. Wang, M.Q. Wang, T. Li, J. Wang, A.M. Abd Ei-Aty, A. Hacımüftüoğlu, Y. She, A dummy molecularly imprinted solid-phase extraction coupled with liquid chromatography-tandem mass spectrometry for selective determination of four pyridine carboxylic acid herbicides in milk, J. Chromatogr., B: Anal. Technol. Biomed. Life Sci. 1108 (2019) 65–72, https://doi.org/10.1016/j.jchromb.2019.01.008.
[22] Y. Zhang, Y. Lu, J. Zhong, W. Li, Q. Wei, K. Wang, Molecularly imprinted polymer microspheres prepared via the two-step swelling polymerization for the separation of lincomycin, J. Appl. Polym. Sci. 136 (2019) 1–7, https://doi.org/10.1002/app.47938.
[23] D. Durce, S. Salah, L. Wang, N. Maes, Complexation of Sn with Boom Clay natural organic matter under nuclear waste repository conditions, Appl. Geochem. 123 (2020), 104775, https://doi.org/10.1016/j.apgeochem.2020.104775.
[24] S.D.M. Colombo, L.B.D.O. Dos Santos, J.C. Masini, G. Abate, Acid/base and complexation properties of humic and fulvic acids isolated from vermicompost, Quim. Nova 30 (2007) 1261–1266, https://doi.org/10.1590/s0100-40422007000500039.
[25] G. Abate, J.C. Masini, Acid-basic and complexation properties of a sedimentary humic acid. A study on the barra bonita reservoir of tietê river, São Paulo state, Brazil, J. Braz. Chem. Soc. 12 (2001) 109–116, https://doi.org/10.1590/S0103-50532001000100015.
[26] E.D. Revellame, D.L. Fortela, W. Sharp, R. Hernandez, M.E. Zappi, Adsorption kinetic modeling using pseudo-first order and pseudo-second order rate laws: a review, Clean. Eng. Technol. 1 (2020), 100032, https://doi.org/10.1016/j.clet.2020.100032.
[27] E.A.O. Pereira, V.F. Melo, G. Abate, J.C. Masini, Adsorption of glyphosate on Brazilian subtropical soils rich in iron and aluminum oxides, J. Environ. Sci. Health Part B Pestic. Food Contam. Agric. Wastes 54 (2019) 906–914, https://doi.org/10.1080/03601234.2019.1644947.
[28] C.H. Giles, D. Smith, A general treatment and classification of the solute adsorption isotherm I. Theoretical, J. Coll. Inter. Sci. 47 (1974) 755–765, https://doi.org/10.1016/0021-9797(74)90252-5.